Tactile Network Resource Allocation enabled by Quantum Annealing based on ILP Modeling

Arthur Witt* , Christopher Körber† , Andreas Kirstädter‡ and Thomas Luu§
*,‡ *Institute of Communication Networks and Computer Engineering, University of Stuttgart*, Stuttgart, Germany
† *Institute of Theoretical Physics II, Ruhr-University Bochum*, Bochum, Germany
§ *Institute for Advanced Simulation (IAS-4) & JARA HPC, Forschungszentrum Jülich*, Jülich, Germany
{arthur.witt, andreas.kirstaedter}@ikr.uni-stuttgart.de, christopher.koerber@rub.de, t.luu@fz-juelich.de

***Abstract*—Agile networks with fast adaptation and reconfiguration capabilities are required for sustainable provisioning of high-quality services with high availability. We propose a new methodical framework for short-time network control based on quantum computing (QC) and integer linear program (ILP) models, which has the potential of realizing a real-time network automation. Finally, we study the approach's feasibility with the state-of-the-art quantum annealer D-Wave Advantage™ 5.2 in case of an example network and provide scaling estimations for larger networks. We embed network problems in quadratic unconstrained binary optimization (QUBO) form for networks of up to 6 nodes. We further find annealing parameters that obtain feasible solutions that are close to a reference solution obtained by classical ILP-solver. We estimate a real-sized network with 12 to 16 nodes require a quantum annealer (QA) hardware with at least 50 000 qubits or more.**

***Index Terms*—integer linear program, quantum annealing, network automation, optical networks, resource allocation**

I. Introduction

A. Motivation

Optical wide-area networks are the backbone for public communication systems like 5G mobile communication and different variants of fixed-access networks. The transport of internet protocol (IP) traffic requires a conversion from electrical to optical signals and vice versa and is realized by power-hungry transceivers within the optical networks. Because traffic volume changes over time, adapting the network configuration to new demands is beneficial. The temporal changes, on the one hand, follow a diurnal profile [6], [7] and, on the other hand, fluctuate within seconds and subseconds [8], [9]. Therefore, the economical adaptive operation of networks requires fast control algorithms for dynamic resource allocation, traffic engineering and restoration. Typically, heuristic methods are used for network reconfiguration [10], [11].

The authors gratefully acknowledge the Jülich Supercomputing Centre for funding this project by providing computing time through the Jülich UNified Infrastructure for Quantum computing (JUNIQ) on the D-Wave Advantage™ quantum system.

This work has been performed in the framework of the CELTIC-NEXT EUREKA project AI-NET ANTILLAS (Project ID C2019/3-3), and it is partly funded by the German Federal Ministry of Education and Research (Project ID 16 KIS 1312).

The authors thank C. C. Chang and D. Willsch for fruitful discussions.

The authors alone are responsible for the content of the paper.

The underlying problem of network resource adaptation is an optimization problem of integer variables under constraints. This kind of problem can be formulated as an integer linear program (ILP). Solving ILPs for network resource allocation can be time consuming, especially if a detailed modeling of the network architecture and operation strategies take place. Therefore, an ILP-based network adaptation in short time periods is difficult to achieve, cf. [5]. In a real network, problems like these are often solved with heuristic or metaheuristic approaches, which allow for a fast solvability at the expense of modeling accuracy and additional effort for the design of the heuristic, cf. [10], [11].

Quantum hardware that leverages the superposition of quantum bits allows performing massively parallel optimization protocols and could possibly overcome the time constraints for short time optimizations. Only through the recent technological progress has it become possible to map feasible optimization problems on quantum hardware. In particular, our work proposes a new ILP-based solution approach for the aforementioned network problem that can be solved on a QA, a form of quantum computing architecture. While solutions obtained on a quantum hardware are not generally guaranteed to be optimal, this problem is an ideal use case for such algorithms as it is only required to obtain better solutions—which can be verified within microseconds.

B. Objectives

We test the feasibility of solving network optimization on quantum hardware. Specifically, we test the feasibility to extract solutions of a non-trivial discrete optimization problem within short time scales. Because today's networks are controlled in a centralized way by software-defined network (SDN), it is possible in principle to incoporate this quantum framework in realistic network configuration setups for traffic engineering and restoration.

We use the new D-Wave Advantage™ 5.2 quantum annealer in Jülich for the evaluation of our network optimizing algorithm. We illustrate the essential steps in the application of the QA to the network problem, and discuss the discovered challenges and restrictions of our approach. Our network scaling study allows us to make quantitative statements related to the feasibility of our approach and QA-related requirements for solving real-world network problems.

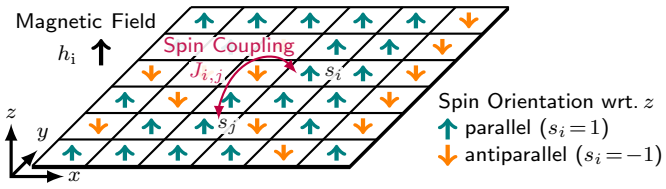

Fig. 1. Visualization of spin configuration in a 2D-lattice (flat material) which is determined by the Ising model (1).

C. Organization of the Work

In Sec. II, we briefly explain the notion of a QA and how an ILP is mapped to the quantum hardware. Furthermore, we address potential constraints and sources of errors which inform our optimization strategy. In Sec. III, we specify the network problem and explicitly derive the formulation of the resource allocation ILP in terms of the QA API. Sec. IV-B, presents our strategy for solving the ILP on the annealer and Sec. IV presents obtained results for the example network topology as well as scaling estimations for larger networks, which we conclude in Sec. V.

II. Preliminaries

A. The Ising model

In physics, the Hamiltonian function is used to derive the equations of motions of a classical system. The Hamiltonian itself represents the total energy of the system. The classical Ising model is described by the Hamiltonian function,

$$\mathcal{H}_{\text{Ising}}(\boldsymbol{s}) = \sum_i h_i s_i + \sum_{i>j} J_{i,j} s_i s_j \ , \tag{1}$$

where $s_i = \pm 1$ are spin projections in the z direction and h_i is an external magnetic field at site i. The coupling between spins at sites i and j is given by $J_{i,j}$. This model describes an array of spins in 2-D, as shown in Fig. 1, and provides a simple representation of ferromagnetism that exhibits a second order phase transition. From a QA perspective, it serves as an objective function to be minimized.

B. Quantum Annealing

The quantum mechanical equivalent of a classical system can be obtained by replacing canonical coordinates and momenta with operators (cannonical quantization). As a consequence, previously commuting expressions may now not be commutable. In case of the Ising model, the spin variables s_i are replaced by spin operators: the pauli matrices $\hat{\sigma}$. The D-Wave Advantage™ system starts initially with a *transverse* Ising model. By the application of external magnetic fields, the annealer adjusts the the time-dependent amplitudes of the Hamiltonian operator in both the x, or transverse, direction and z direction, respectively,

$$\hat{\mathcal{H}}_{\text{QPU}} = \frac{A(s)}{2}\hat{\mathcal{H}}_{\text{initial}} + \frac{B(s)}{2}\hat{\mathcal{H}}_{\text{problem}} \tag{2}$$

$$\hat{\mathcal{H}}_{\text{initial}} = \sum_i \hat{\sigma}_{\text{x}}^{(i)} \tag{3}$$

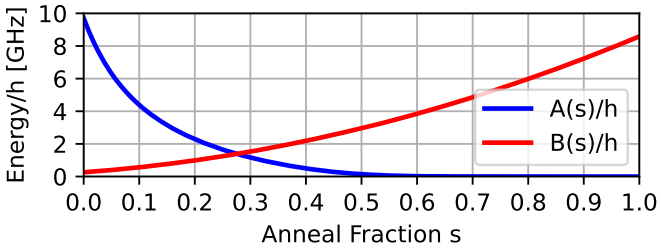

Fig. 2. Energy variation of $A(\text{s})$ and $B(\text{s})$ to perform the annealing within the D-Wave Advantage™ 5.2 acc to (2). Energy values are normalized by the Planck constant $h = 6.62 \cdot 10^{-34}$Joules based on the relation $E = hf$. The anneal fraction s will be varied over time within the annealing duration to perform either a standard, paused, quenched, reverse or individual annealing schedule.

$$\hat{\mathcal{H}}_{\text{problem}} = \sum_i h_i \hat{\sigma}_{\text{z}}^{(i)} + \sum_{i>j} J_{i,j} \hat{\sigma}_{\text{z}}^{(i)} \hat{\sigma}_{\text{z}}^{(j)} \ . \tag{4}$$

Here $\sigma_{x,z}$ represent Pauli sigma matrices. Because the spin projections in the x and z directions do not commute, this system must be solved quantum mechanically and is therefore also known as the *quantum* Ising model. The external fields depend on time. Initially $A(\text{s}) \gg B(\text{s})$ at time $t = 0$ corresponding to an annealing fraction $\text{s} = 0$, but adiabatically changes to $B(\text{s}) \gg A(\text{s})$ at some anneal time $t = t_f$ corresponding to an annealing fraction $\text{s} = 1$, as shown in Fig. 2. After time t_f the system has annealed to purely $\hat{\mathcal{H}}_{\text{problem}}$, and since $\hat{\sigma}_z$ has either ± 1 expectation values, this is identical to the classical Ising model in Eq. (1).

C. Solving ILPs on Quantum Annealer

A method for solving integer linear programs (ILPs) on quantum annealers was published firstly in [1]. In the following we shortly recap this method to point out the required steps of this problem mapping strategy. The programming of D-Wave's quantum annealer requires the representation of the problem as a QUBO problem for bit vectors $\boldsymbol{\psi} \in \{0,1\}^N$

$$X^2(\boldsymbol{\psi}) = \boldsymbol{\psi}^\top \boldsymbol{Q} \boldsymbol{\psi} \, . \tag{5}$$

The annealer aims at finding the optimal bit vector $\boldsymbol{\psi}$ which minimizes the objective function X^2.

In the first step, we have to specify an ILP formulation of an optimization problem, e.g. the proposed network problem. The further steps define how it is mapped to the QUBO formalism.

ILPs are defined by an objective function, a set of K constraints and M integer variables $x_m \geq 0$, shortly denoted as vector $\boldsymbol{x} \in \mathbb{N}^M$. The objective function defines the optimization target in the form

$$\boldsymbol{c}^\top \boldsymbol{x} \to \min \tag{6}$$

with the cost weights $\boldsymbol{c}^\top \in \mathbb{R}^M$. The constraints are given in the form of equalities or inequalities according to

$$\boldsymbol{A}\boldsymbol{x} + \boldsymbol{b} \leq 0 \tag{7}$$

with constant values $\boldsymbol{b} \in \mathbb{R}^K$ and the matrix $\boldsymbol{A}$ that contains the linear weights $A_{k,m} \in \mathbb{R}^{K,M}$ for all constraints of the

ILP. Typically, for solving ILPs, the inequality constraints are transformed to equality constraints by introducing integer slack variables $\boldsymbol{s} \in \mathbb{N}^K$ as follows

$$\boldsymbol{A}\boldsymbol{x} + \boldsymbol{b} \leq 0 \Leftrightarrow \boldsymbol{A}\boldsymbol{x} + \boldsymbol{b} + \boldsymbol{s} = \boldsymbol{0} \; . \tag{8}$$

Introducing a sufficiently large penalty factor p, the objective function and constraints can be combined to a quadratic optimization of objective and penalty

$$X^2(\boldsymbol{x}, \boldsymbol{s}) = \boldsymbol{c}^\top \boldsymbol{x} + p \left\| \boldsymbol{A}\boldsymbol{x} + \boldsymbol{b} + \boldsymbol{s} \right\|^2 \rightarrow \min \; . \tag{9}$$

Given that the penalty term p is large enough, the combined minimization of X^2 in terms of $\boldsymbol{x}, \boldsymbol{s}$ returns the optimal vector $\boldsymbol{x}_0$ which minimizes X^2 under the constraints.

To map the integer quadratic optimization problem to a binary QUBO problem, we introduce the matrices $\boldsymbol{Z}$ such that

$$\boldsymbol{x} = \boldsymbol{Z}_x \boldsymbol{\psi}_x, \quad \boldsymbol{s} = \boldsymbol{Z}_s \boldsymbol{\psi}_s \, . \tag{10}$$

We thus find the QUBO problem of the form

$$X^2(\boldsymbol{q}) = \boldsymbol{c}^\top \boldsymbol{Z}_x \boldsymbol{q}_x + p \left\| \boldsymbol{A}\boldsymbol{Z}_x \boldsymbol{q}_x + \boldsymbol{b} + \boldsymbol{Z}_s \boldsymbol{q}_s \right\|^2 \rightarrow \min \, . \tag{11}$$

In terms of the matrix formulation required by the D-Wave API, this becomes

$$X^2(\boldsymbol{\psi}) = \boldsymbol{\psi}^\top \boldsymbol{Q} \boldsymbol{\psi} + C \tag{12}$$

with $$\boldsymbol{Q} = p \begin{bmatrix} \boldsymbol{Q}_{xx} & \boldsymbol{Q}_{xs} \\ \boldsymbol{Q}_{sx} & \boldsymbol{Q}_{ss} \end{bmatrix}, \quad C = p \left\| \boldsymbol{b} \right\|^2$$

$$\begin{aligned} \boldsymbol{Q}_{xx} &= \boldsymbol{Z}_x^\top A^\top A \boldsymbol{Z}_x + \mathrm{diag} \left\{ \left(2\boldsymbol{b}^\top A + \frac{1}{p} \boldsymbol{c}^\top \right) \boldsymbol{Z}_x \right\} \\ \boldsymbol{Q}_{xs} &= \boldsymbol{Q}_{sx}^\top = \boldsymbol{Z}_x^\top A^\top \boldsymbol{Z}_s \\ \boldsymbol{Q}_{ss} &= \boldsymbol{Z}_s^\top \boldsymbol{Z}_s + 2 \mathrm{diag} \left\{ \boldsymbol{Z}_s^\top \boldsymbol{b} \right\} \; . \end{aligned} \tag{13}$$

Matrix $\boldsymbol{Q}$ is symmetric ($\boldsymbol{Q}^\top = \boldsymbol{Q}$), which is directly visible in their definition (13). Further, it is used only in the form $\boldsymbol{\psi}^\top \boldsymbol{Q} \boldsymbol{\psi}$ to determine a energy value. This allows one to transform $\boldsymbol{Q}$ to a triangular matrix $Q_{\mathrm{Triag}} = \mathrm{tril}\{Q\}^\top + \mathrm{triu}\{Q\}$. Function $\mathrm{tril}\{\cdot\}$ selects the triangular part below the main diagonal of a matrix, and $\mathrm{triu}\{\cdot\}$ the upper triangular part inclusive the main diagonal. As the constant C is independent of the solution vector $\boldsymbol{\psi}$, it does not affect the location of the minimum.

The Ising model wave function components σ_i are related to components of the QUBO bit vectors $\boldsymbol{\psi}$ by a linear shift $\sigma_i = 2\psi_i - 1$. Equating respective objective functions allows to identify the mapping from QUBO matrix to the Ising Hamiltonian in matrix form

$$\boldsymbol{\psi}^\top \boldsymbol{Q} \boldsymbol{\psi} = \boldsymbol{\sigma}^\top \boldsymbol{J} \boldsymbol{\sigma} + \boldsymbol{h}^\top \boldsymbol{\sigma} + g \Rightarrow \begin{cases} \boldsymbol{J} &= \frac{1}{4} \boldsymbol{Q}_0 \\ \boldsymbol{h} &= \frac{1}{2} \boldsymbol{q} + \frac{1}{2} \boldsymbol{1}^\top \boldsymbol{Q}_0 \\ g &= \frac{1}{4} \boldsymbol{1}^\top \boldsymbol{Q}_0 \boldsymbol{1} + \frac{1}{2} \boldsymbol{1}^\top \boldsymbol{q} \end{cases} . \tag{14}$$

These equations were obtained by expressing QUBO vectors as Ising vectors, defining the traceless part of the QUBO $\boldsymbol{Q}_0 = \boldsymbol{Q} - \mathrm{diag}\{\boldsymbol{q}\}$ and $\boldsymbol{q} = \mathrm{diag}^{-1}\{\boldsymbol{Q}\}$ (since $\boldsymbol{J}$ is not allowed to have diagonal components), and using that $\psi_i^2 = \psi_i$. Here $\mathrm{diag}\{\cdot\}$ transforms a vector into a diagonal matrix and $\mathrm{diag}^{-1}\{\cdot\}$ extracts the diagonal part of the matrix as a vector. $\boldsymbol{1}$ is a vector where each component is one.

D. Embedding

A QUBO can be viewed as a weighted graph where nodes correspond to qubits, edges represent the coupling of two qubits, and the weight of edges the strength of the coupling. Because the hardware topology may have a different connectivity as required by the QUBO, several hardware qubits must be chained together to form a single logical qubit (nodes of the QUBO graph). Generally, problems which have small chains while using the entire hardware are found to be more optimal [12]. As such, finding valid embeddings is an essential constraint for being able to solve a problem. This embedding constraint is affected by the number of qubits present in the formulation (i.e., dimension of the QUBO matrix) and the density of the QUBO matrix (number and locations of non-zero entries).

This pre-processing procedure, e.g. finding a valid hardware embedding for the given problem, must be performed before submitting problems to the annealer. Depending on the problem size, finding a valid embedding may take several hours on a single CPU. However, since an embedding is a map from QUBO nodes to hardware topology nodes, which does not depend on the relative coupling strengths, it is possible to export valid embeddings which are reusable for a larger set of problems. Thus, the expensive part of finding an embedding must be performed only once for a class of problems.

E. Sources of Errors and Statistics

In principle, optimal solutions of the QUBO problem are automatically optimal solutions to the network ILP. However, solutions returned by the QA may be non-optimal because of errors during the annealing process. For example, depending on the specification of the annealing schedule, non-adiabatic transitions from the ground state to an excited state may occur if the annealing happens too fast. Especially, if energy gaps between excited and ground states are small.

If the annealing happens too slowly, temporal or thermal decorrelation of qubits may occur so that qubits may freeze in position independent of the problem Hamiltonian. On the other hand, it may not be possible to set up the problem on the hardware—even if a valid embedding was found. For example, if qubit chains are too long, they potentially break such that one solves a different problem. Or, since the magnetic fields generated by the hardware are only manipulated with finite precision, the resolution of the QUBO entries may exceed the magnetic field precision. It is *a priori* not known if these problems may occur during an annealing schedule. For a given problem setup, one must therefore perform multiple annealing schedules and post-process the results to identify valid solutions. This procedure provides distributions of solutions with varying degrees of quality.

III. Resource Allocation in Wide Area Networks

A. Problem Description

An optical network is typically composed of transceiving terminals and optical cross connects (OXC) at the network nodes and optical line systems at the edges (between nodes) of

the network. At the terminals, transponders are equipped for transmission and reception of optical signals. This includes the power-hungry conversion of signals from the electrical to optical domain or the other way round. Optical line systems are composed of multiplexers for signal combining, and a sequence of fiber spans and amplifiers to increase the optical transmission reach. The combination of signals inside a multiplexer is performed along the concept of dense wavelength division multiplexing (DWDM), i.e., the fiber bandwidth is divided into a finite number of channels with 50GHz bandwidth each. An optical channel can be identified by its central wavelength and is assigned to an optical fiber located at a specific network edge. An optical circuit enables an unidirectional traffic flow in the optical domain. It consists of a single optical channel or a subsequent sequence of optical channels and is terminated with two transponders, one at the source and one at the target node.

We will consider a network architecture that is restricted as follows:

- **Singe Rate System:** All transponders operate at a fixed bandwidth. Optical channels provide a signal data rate of 100 Gbit/s. An optical circuit is a sequence of optical channels allocated at different network edges. It has the same bandwidth as an optical channel and a maximal optical reach of 1000 km. Optical circuits are terminated by two transponders corresponding to transmitter and receiver.
- **Colorless Wavelength Assignment:** Depending on the required data rate one or more optical channels resp. wavelengths are allocated. It is not required to select a specific wavelength (e.g., for the provisioning of wavelength continuity along a sequence of network edges) as the OXCs, present at all nodes, provide a wavelength conversion in the optical domain during the forwarding process.

An essential part of the network operation is the on-demand or regularly traffic engineering. This process considers:

- **Traffic Routing:** For realizing a traffic flow between two nodes, a sequence of links resp. nodes, i.e. a transmission path, has to be selected. Typically, the shortest path is selected as it provides normally the shortest latency. However, considering alternative paths increases the amount of combinations for possible traffic flow migrations and could allow network resources to be used more efficiently.
- **Resource Allocation:** Establishing a transmission path requires the activation of optical circuits which includes the allocation of optical channels per traversed network edge and transponders. We considered optical channels that are not limited to massive over-provisioning of fibers. The expensive transponders are limited per node and can be used for transmission or reception.

The allocation of resources in wide-area networks can be interpreted as a combinatorial problem: In a preparation phase, a set of resources and traffic routes has to be defined. Then, the network's resource utilization can be optimized by choosing a subset that fulfils the conditions of a proper network operation. These steps will be explained in detail in the following Sec. III-B and III-C. Finally, we want to minimize the amount of utilized optical circuits and implicitly the amount of active transponders. This will lower the overall energy consumption of the network.

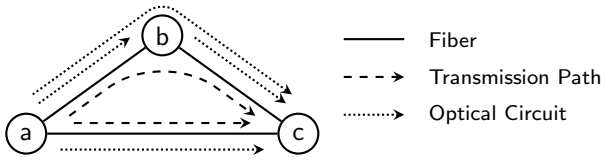

Fig. 3. Definition of transmission path and circuits. For data transport between node a and c, two transmission paths are possible. The transmission path a–b–c can be realized a) by a direct circuit a–b–c, that is bypassing node b in the optical domain, or b) by the sequence of circuits (a–b, b–c), which requires two additional transponders for signal conversion at node b.

B. Generation of Path and Circuit Variations

A traffic flow between two nodes $u \in V$ and $v \in V$, also named as unidirectional demand d for the disjunct node pair (u, v) with $u \neq v$, requires resources in a network to be realized. V is the set of all network nodes, and D the set of all demands in the network. As depicted in Fig. 3, a transmission path is defined by a sequence of nodes resp. edges of the network graph, that provides a connectivity between the source and target node of an unidirectional demand. The realization of a transmission path is done by a sequence of optical circuits.

First of all, we generate a set of circuits C that includes all direct circuits, i.e. circuits that traverse a single network edge, and a finite number of alternatives for them if possible. We must therefore consider the optical reach of a circuit and the restrictions of its topology.

Based on a shortest path search, we can identify a set of one or more loop-free paths L_d per demand d, that are listed by their distance in ascending order. As a circuit can also transport a combination of different traffic flows by migration, it might be beneficial if some of the transmission paths are realized by a sequence of rather short circuits, which increases the flexibility for migration. Therefore, we compute a set $R_{d,l}$ of possible circuit realizations $r \in R_{d,l}$ with circuits from C_{temp} for each transmission path $l \in L_d$. The first circuit realization in $R_{d,l}$ contains a pattern with the shortest possible circuits, i.e. they traverse only a single edge of the network. The second realization uses a pattern with a minimal amount of circuits, followed by some intermediate circuit pattern. For simplicity we will define the union set T_d, where $t_d \in T_d$ are all circuit realization variants for traffic flow d, and the total union set T according to

$$T_d = \bigcup_{l \in L_d} R_{d,l} \quad \text{and} \quad T = \bigcup_{d \in D} T_d. \tag{15}$$

In the case that not all circuits of C are used in T, we delete the not required circuits from set C.

C. ILP Form

ILPs for resource allocation and service provisioning in wide area networks are often used as a reference method providing exact solutions for comparison with newly developed heuristic or meta-heuristic algorithms. Sometimes they are also used to study the possible benefit of new network operation strategies. Some examples are given in [2], [4] where the reduction of over-provisioned quality of services in networks was studied.

To study the applicability of solving a network resource allocation problem on quantum annealers we define the following terms based on [2], whereas the traffic volume h_d of a demand d is varying over time. Nevertheless, for the ILP it is considered as a constant. The variations over time are considered by frequently solving the ILP with updated values of h_d.

Variables:

- $g_{t_d} \in \{0,1\}$: path selector, i.e., g_{t_d} equals 1 if a transmission path for demand d is realized by circuit configuration $t_d \in T_d$.
- $w_c \in \mathbb{N}$: the number of active, parallel circuits on circuit path c.

Constants:

- $\xi \in \mathbb{R}$: the data rate of a single optical circuit.
- $\eta_v \in \mathbb{N}$: the amount of transceivers installed at node v.
- $\rho_{c,t_d} \in \{0,1\}$: indicates whether circuit configuration t_d uses circuit path c.
- $\varphi_{v,c} \in \{0,1\}$: indicates whether node v is the source or target node of circuit path c.
- $h_d \in \mathbb{R}$: traffic volume of demand d.

Constraints:

$$\sum_{t_d \in T_d} g_{t_d} = 1 \qquad \forall d \in D \tag{16}$$

$$-w_c + \sum_{d \in D} \sum_{t_d \in T_d} \rho_{c,t_d} \cdot \frac{h_d}{\xi} \cdot g_{t_d} \leq 0 \qquad \forall c \in C \tag{17}$$

$$\sum_{c \in C} w_c \cdot \varphi_{v,c} \leq \eta_v \qquad \forall v \in V \tag{18}$$

Objective:

$$\sum_{c \in C} w_c \;\rightarrow\; \min. \tag{19}$$

Equation (16) ensures that a demand is routed on exactly one path. The constraint (17) ensures that enough circuits are activated depending on the chosen paths. Constraint (18) activates a sufficient amount of transceivers to accommodate the active optical circuits. Finally, the objective (19) minimizes the number of active circuits and therefore also the number of active transceivers.

D. Matrix Form

An intermediate step of the ILP to QUBO mapping described in Sec. II-C is the reformulation of the ILP in matrix form. Thus, the network allocation ILP given in Sec, III-C is equivalent to

$$A = \begin{bmatrix} \boldsymbol{G}^{|D|\times|T|} & \boldsymbol{0}^{|D|\times|C|} \\ \boldsymbol{H}^{|C|\times|T|} & -\mathbb{I}^{|C|\times|C|} \\ \boldsymbol{0}^{|V|\times|T|} & \boldsymbol{\varphi}^{|V|\times|C|} \end{bmatrix}, \boldsymbol{b} = -\begin{bmatrix} \boldsymbol{1}^{|D|} \\ \boldsymbol{0}^{|C|} \\ \boldsymbol{\eta}^{|V|} \end{bmatrix}, \boldsymbol{s} = \begin{bmatrix} \boldsymbol{0}^{|D|} \\ \boldsymbol{s}_{\mathrm{c}}{}^{|C|} \\ \boldsymbol{s}_{\eta}^{|V|} \end{bmatrix},$$

$$\boldsymbol{x} = \begin{bmatrix} \boldsymbol{g}^{|T|} \\ \boldsymbol{\omega}^{|C|} \end{bmatrix}, \; \boldsymbol{c}^{\top} = \begin{bmatrix} \boldsymbol{0}^{|T|} & \boldsymbol{1}^{|C|} \end{bmatrix}. \tag{20}$$

The term $|\cdot|$ in the superscript of the matrices defines the size of the used sets C, D, T and V and defines the matrix's dimensions. Vector resp. matrix $\mathbf{0}$ contains only zero values, and entries of $\mathbf{1}$ are all one. $\mathbb{I}$ is a identity matrix.

Column vector $\boldsymbol{x}$ contains the ILP's variables $\boldsymbol{g} = [g_{t_d}] \in \{0,1\}^{|T_d|}$ and $\boldsymbol{\omega} = [\omega_c] \in \{\mathbb{N} \leq \omega_{\max}\}^{|C|}$. $\boldsymbol{c}$ contains the weights to realize the cost function (19) of the ILP.

The rows of $\boldsymbol{A}$, $\boldsymbol{b}$ and $\boldsymbol{s}$ are ordered according to the constraints of the ILP. The first row with matrix

$$\boldsymbol{G} = \begin{bmatrix} \boldsymbol{1}^{1\times|T_1|} & \boldsymbol{0}^{1\times|T_2|} & \dots & \boldsymbol{0}^{1\times|T_{|D|}|} \\ \boldsymbol{0}^{1\times|T_1|} & \boldsymbol{1}^{1\times|T_2|} & \dots & \boldsymbol{0}^{1\times|T_{|D|}|} \\ \vdots & \vdots & \ddots & \vdots \\ \boldsymbol{0}^{1\times|T_1|} & \boldsymbol{0}^{1\times|T_2|} & \dots & \boldsymbol{1}^{1\times|T_{|D|}|} \end{bmatrix} \tag{21}$$

describes the possible path selection according to (16). The second row describes how the traffic volume h_d per demand d are distributed over the set of circuits C, cf. (17). As h_d is typically a real number we perform a quantization, defined by a number of digits $a \in \mathbb{N}$, and normalization to the single circuit capacity ξ in the form

$$\overline{h}_d = \left\lceil \frac{h_d * 2^a}{\xi} \right\rceil \cdot \frac{1}{2^a}. \tag{22}$$

Expression $\lceil \cdot \rceil$ indicates a rounding to the next larger integer value. Together with $\boldsymbol{\rho}_d = [\rho_{c,t_d}] \in \{0,1\}^{|C|\times|T_d|}$, describing the existence of a circuit c inside a circuit configuration t_d for demand d, the matrix H can be given as

$$\boldsymbol{H} = \begin{bmatrix} \overline{h}_1\boldsymbol{\rho}_1 & \overline{h}_2\boldsymbol{\rho}_2 & \dots & \overline{h}_{|D|}\boldsymbol{\rho}_{|D|} \end{bmatrix} \tag{23}$$

The last row of $\boldsymbol{A}$,$\boldsymbol{b}$ and $\boldsymbol{s}$ considers the limited amount of installed transceivers $\boldsymbol{\eta} = [\eta_v] \in \{N \leq \eta_{\max}\}^{|V|}$ per node v, cf. (18). Thereby, $\boldsymbol{\varphi} = [\varphi_{v,c}] \in \{0,1\}^{|V|\times|C|}$ describes whether a transceiver at node v is connectable to a circuit c.

The slack vector $\boldsymbol{s}$ has an all-zero block entry in the first block as (16) is an equality constraint. $\boldsymbol{s}_{\mathrm{c}} = [s_c] \in \{\mathbb{N} \leq a\}^{|C|}$ and $\boldsymbol{s}_{\eta} = [s_{\eta}] \in \{\mathbb{N} \leq \eta_{\max}\}^{|C|}$ are variables with a limited integer space. A set of results, obtained by following the procedure of Sec. II-C and the final optimization of the QUBO matrix $\boldsymbol{Q}$ on a quantum annealer, have to be checked according to their feasibility. The feasibility is given if $\boldsymbol{g}$ and $\boldsymbol{\omega}$ fulfill the conditions

$$\boldsymbol{G}\boldsymbol{g} \overset{!}{=} \boldsymbol{1}, \quad \boldsymbol{H}\boldsymbol{g} - \boldsymbol{\omega} \overset{!}{\leq} \boldsymbol{0}, \quad \boldsymbol{\varphi}\boldsymbol{\omega} - \boldsymbol{\eta}, \quad \overset{!}{\leq} \boldsymbol{0} \tag{24}$$

TABLE I

SELECTED VALUES FOR $\eta_{\max}$, LIMIT OF INSTALLED TRANSCEIVERS PER NODE, AND THE MAXIMAL AMOUNT $\omega_{\max}$ OF PARALLEL CIRCUITS AT CIRCUIT PATH c IN DEPENDENCE OF THE NETWORK SIZES $|V|$.

$\lvert V\rvert$	3–4	5–7	8–11	12	13–16
$\eta_{\max}$	15	31	63	63	127
$\omega_{\max}$	3	3	3	7	7

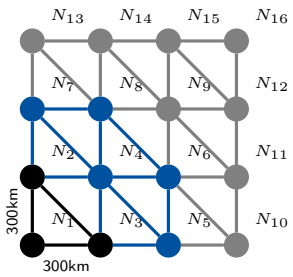

Fig. 4. Topology of a growing network. (●): smallest network with 3 nodes, (●): exemplary extension to a 8 node network, (●) maximal considered extension.

IV. FEASIBILITY STUDY

A. Network Scenario

For studying the performance of our approach and the scalability in terms of the network size, a growing network topology is used as depicted in Fig. 4. The nodes of this topology are added in ascending order starting with a 3 node network in the lower left corner. The edges are added correspondingly. The vertical and horizontal distance between neighboring nodes is set to 300 km. A set of topologies with $|V| \in \{3, 4, \ldots, 8\} \subset \mathbb{N}$ was studied to test the feasibility of finding an embedding. The three node network was studied to analyze the probability for the annealer to find feasible solutions.

The network loads are defined by a demand matrix with values h_d for traffic demands between the pairs of disjunct nodes $d \in D$. The values for h_d are samples of a normal distribution $\mathcal{N}(\mu, \sigma)$ with $\mu = 75$ and $\sigma = 20$.

B. Solution Strategy

The solution strategy for reaching a tactile resource allocation in wide area networks can be stated as follows.

1) For a fixed network problem, we generate QUBOs with different penalty terms, qubit permutations, and number of slack digits (affecting the shape and values of the QUBOs while solving the same problem).
2) We heuristically search different embeddings for each class of QUBO (i.e., with the same dimension and structure).
3) We submit the QUBO with varying annealing meta parameters (i.e., chain strength, total annealing time, annealing schedules, and more).
4) We post-process obtained solutions and classify them by feasibility (solution or x-components fulfill the constraints), QUBO energy (value of $\boldsymbol{\psi}^\top \boldsymbol{Q}\boldsymbol{\psi} + C$), solution energy (value of $\boldsymbol{c}^\top \boldsymbol{x}$; i.e., QUBO energy ignoring the penalty part) and number of occurrences per time to solution.

TABLE II

NUMBER OF 1000 SAMPLES PER PENALTY TERM AND ANNEALING SCHEDULE. GREEN ENTRIES FOUND FEASIBLE SOLUTIONS.

t_{ps}/p	1	2	4	8	16	1000
1μs	600		170			48
50μs			117			
100μs			99			
100μs @ 0.35 + 20μs	50	50	50	50	50	
100μs @ 0.50 + 20μs	50	50	60	50	50	
500μs			30			
1000μs			17			

In total, we have gathered a total of $N_\psi = 5.1 \cdot 10^7$ samples distributed over $N_s = 3.3 \cdot 10^3$ submissions for in total $N_E = 40$ different embeddings resulting in over $N_c = 2 \cdot 10^3$ distinct parameter combinations. We have varied parameters which we found to have a larger impact on a logarithmic scale. In particular, these were the annealing schedules and the penalty term. The annealing schedules were varied in the range of an annealing time per sample of $t_{ps} = 1, 50, 100, 500, 1000\mu s$ and a stop schedule where, for $100\mu s$, the annealing was stopped at an interval of $s = 0.35, 0.5$ (allowing for more transverse Ising model interaction time). The penalty term was varied from $p = 1, 2, 4, 8, 16, 1000$. See also Tab. II for the number of samples per parameter configuration. Table cells highlighted with a green color are parameter combinations which returned feasible solutions.

All further run parameters and specifications are logged to a database and openly accessible under [1].

C. Hardware Limitations of the used Quantum Annealer

As mentioned in Sec. II-D the embedding of a QUBO to the D-Wave's quantum annealer is an important step. The optimization problem size, i.e. the dimension of the QUBO, can be expressed by the number of required logical qubits. As logical qubits are realized by a coupled chain of physical qubits, the average chain length can be seen as a metric for the efficiency of an embedding. Fig. 5 shows this metric for 3 to 6 node networks. The varied number of digits a changes the numerical accuracy of the ILP's constraint (17), and changes therewith the problem size. We observe that the average chain length follows a linear law of $2.13 \cdot |V|$. This can be used for extrapolation to larger network sizes, as the QUBO embedding for larger network with more than 6 nodes are not achievable at the D-Wave Advantage 5.2™ for now.

Fig. 6 shows the resulting relative hardware utilization of the quantum annealer for network problems with 3 to 16 nodes. The D-Wave Advantage 5.2™ provides in total 5 600 physical qubits and roughly 40 100 coupling elements. This marks the 100% line of hardware utilization. The amount of required logical qubits increases with the network size

[1] **Open Data Access:** https://jugit.fz-juelich.de/qnet-public/home/

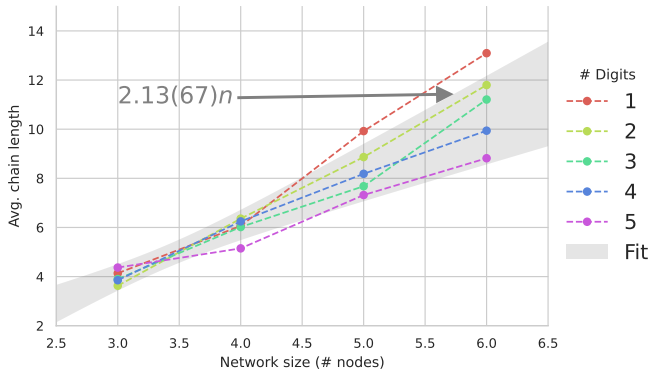

Fig. 5. Average chain length (physical qubits needed to form a logical qubit) depending on the number of nodes in the network and digits required to reperesent demands. The grey band represents a one-parameter fit with propagated uncertainties.

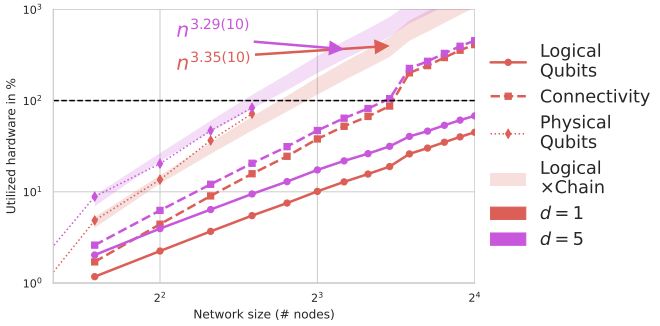

Fig. 6. Hardware utilization of problem depending on problem size. The hardware utilization is expressed by the logical qubits (filled circles) corresponding to the dimension of the QUBO (at most 5.6k qubits for a perfect embedding), the connectivity of the QUBO (squares) corresponding to non-zero entries in the QUBO (at most 40.1k), and physical qubits (diamonds) corresponding to logical qubits times the average chain length (at most 5.6k qubits). Results are displayed for the best scaling using a demand float precision of one bit (brown) and the most precise scaling with five bit precision (purple).

in a range from 66 to 3822, i.e. 1.1% to 66.4%. Further, the QUBOs of the network problems require a connectivity in the range of 684 to 182110, i.e. these are the non-zero elements of $\boldsymbol{Q}$. The amount of maximal available couplers is already exceeded for a network of 12 nodes. As chains of qubits must be built for a proper mapping between logical and physical qubit structure, the amount of physical available qubits is already exceeded for networks with 7 or more nodes. The required amount of physical qubits can be obtained by multiplication of the average chain length and amount of logical qubits, e.g. the 6 node network with 5 digit accuracy has $532 \times 8.8 = 4682$ physical qubits. We summarize, that the embedding of network problems in QUBO form into the D-Wave's quantum annealer is constrained by the number of physical qubits or the connectivity of individual qubits. Increasing the problem accuracy increases the problem size and therefore the required QPU hardware. This effect is not as strong as adding further nodes to a network. Extrapolation of the physical qubit curve in Fig. 6 allows us to estimate how large a QPU in terms of physical qubits for real network problems should be—**at least 10 times more physical qubits are required to operate a wide-area network with a reliable size of 12 to 16 nodes by quantum annealing.** An increase of individual qubit's connectivity would also enable access to larger networks, which is however more difficult to quantify.

D. Results for a 3-Node Network Problem

Based on a 3 node network problem we study the solvability and its dependence on annealing parameters, numerical accuracy and various embeddings. Fig. 7 shows the energy distribution of Eq. (12) for solution vectors obtained by the annealing process in a summary over the various parameter settings. Compared to a random bit guessing approach we observe that quantum annealing provides solution vectors with significantly lower energy values that follow a different distribution.

A more detailed view can be given by analyzing the feasibility, determined by evaluating Eq. (7) post anneal, of

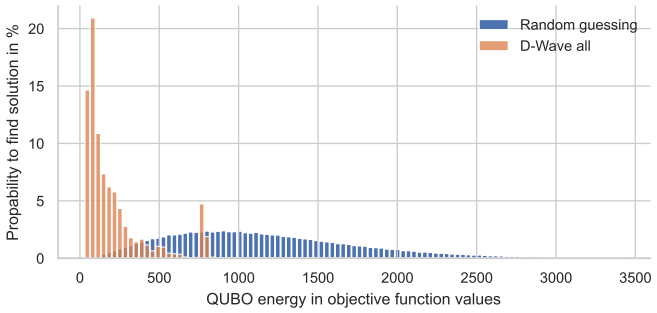

Fig. 7. Probability spectrum of the shifted QUBO objective function values (Eq. (12)) for three-node problem. Displayed probability values correspond to all obtained D-Wave samples independent of the parameter setup and feasibility of the solution (orange) and to randomly sampled integers (blue) for 10^6 samples. The propability is defined as the number of samples within a bin divided by the number of all obtained samples; for each category respectively.

solution samples and evaluation of the finally obtained cost value according to Eq. (6).

A more detailed view can be seen by analyzing the feasibility of solution samples, determined by evaluating eq. (7) post anneal, and evaluation of the final cost value according to eq. (6). Fig. 8 shows the amount (white numbers) of obtained feasible solutions per integer cost values. **The best solution we have found, corresponding to a cost value of** 8**, is one cost step appart from the best reference solution with a cost of** 7**.** The results can be further grouped according to the applied annealing times. It can be observed, that results within the category of a $100\mu s$ annealing duration are better than for the $1\mu s$ case. **Overall, feasible solutions are very rare if it is compared with all obtained samples. This obtained ratio lays below** 1.3×10^{-5} and determines the values of the y-axis of Fig. 8. At this point, it is not possible for us to disentangle if the choice of the penalty term, the annealing schedule, other paramters, or their interplay are responsible for the qualtiy and frequency of the optimal solution within a suitable region.

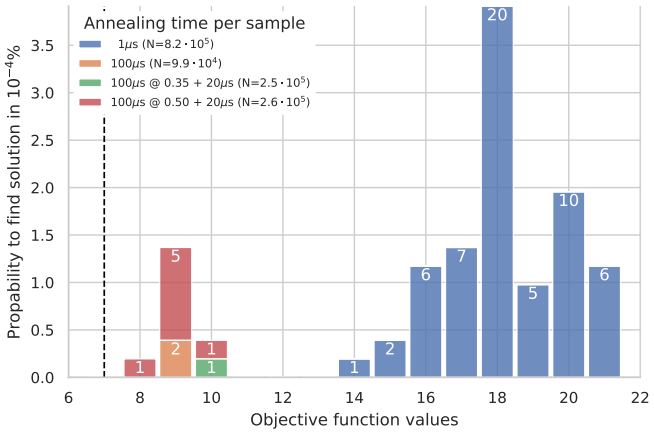

Fig. 8. Probability spectrum of the ILP objective function values (Eq. (6)) for three-node problem obtained by the annealer. Solutions are classified as feasible solutions in post-processing by evaluating (Eq. (24)). The propability is defined as the number of feasible samples for an objective value divided by the number of all obtained samples over all submits (including parameter configurations which did not find feasible solutions). The samples are categorized by different annealing schedules, specified by the annealing time per sample (without overhead), and the number within the bars is the count for a given category. The dashed line is a known reference solution (with value 7).

V. Conclusion and Outlook

We proposed an algorithmic approach relying on the cutting-edge technology of quantum computing for the optimization of resource utilization in SDN-controlled optical wide-area networks. The optimization problem is modelled by an ILP, translated in several steps to a QUBO, which can be solved on a quantum annealer like the D-Wave Advantage™ 5.2. The algorithm can be used for traffic engineering, resource allocation and restoration. At the current stage, feasible reconfigurations for a three-node problem can be obtained every minute or more frequently (defined by chance to find a feasible solution and samples generated over an effective run time). As quantum computing can be superior against classical computing, demonstrated in [15], a further speed-up might be achievable by newer generations of quantum computers or a problem specific QPU, such that network reconfiguration within seconds or below might be possible. Our feasibility study shows that the proposed network problem for up to 6 nodes can be embedded on the D-Wave QPU. We estimate that the amount of physical qubits, assuming the same qubit connectivity, should be in the range of 50 000 or above to optimize networks in reasonable sizes (12 to 16 nodes). Further, we studied the quantum-based solvability of a 3 node network. Compared to a random guessing method, solutions obtained by the quantum annealer show a significant lower energy on average. Solution vectors are checked for feasibility and compared with a reference solution obtained by CPLEX (classical ILP-solver). We showed that feasible solutions with cost values close to the reference solution are obtainable. We discovered that a setting with penalty of 4 and annealing time of 100μs achieved the best results. We see indications that some annealing parameter configurations have a higer chance to return feasible solutions—potentially allowing to find feasible solutions within less than a minute of run time. The parameter variations for the annealing process has to be studied further as the current solution set represents only an empirical sample set which does not not allow one to formulate strong statement on statistical correlations. iT Finally, as larger Ising model based solvers with up to 100 000 qubits [14] are in the reach, embedding 12 to 16 node networks seems realistic in the near future. It remains to be shown that obtaining feasible solutions within a reasonable time is possible for such larger networks. This is the focus of our ongoing research. If succesfull, the proposed approach for network optimization has the potential to have a large impact on how networks are operated in the future enabling real-time network automation.

References

[1] C. C. Chang, C.-C. Chen, C. Körber, T. S. Humble, J. Ostrowski. “Integer Programming from Quantum Annealing and Open Quantum Systems”. [arXiv:2009.11970]

[2] T. Enderle, A. Witt, and F. Christou. “Delay-Differentiated Routing in Meshed Backbone Networks”. *Proceedings of the 21st ITG-Symposium in Photonic Networks 2020*, pp. 20–27, Nov. 2020.

[3] C. C. Chang, C. Körber, A. Walker-Loud. ”EspressoDB: A scientific database for managing high-performance computing workflow”. *J.Open Source Softw. 5 (2020) 46, 2007*, [arXiv:1912.03580]

[4] U. Bauknecht, T. Enderle, and A. Witt. “Reduction of Delay Overfulfillment in IP-over-DWDM Transport Networks”. *Proceedings of the 23rd Conference on Optical Network Design and Modeling (ONDM 2019)*, LNCS 11616, pp. 528–539, Feb. 2020. doi:10.1007/978-3-030-38085-4_45

[5] M. Tomatore, G. Maier, and A. Pattavina. “WDM network optimization by ILP based on source formulation”. *Proceedings. Twenty-First Annual Joint Conference of the IEEE Computer and Communications Societies*. vol. 3. pp. 1813–1821, 2002. 10.1109/INFCOM.2002. 1019435.

[6] T. Enderle, u. Bauknecht. ”Modeling Dynamic Traffic Demand Behavior in Telecommunication Networks”. *Proceedings of the 19th ITG-Symposium in Photonic Networks 2018*, pp. 18–25, 2018

[7] R. Protzmann, et. al. ”Large-scale Modeling of Future Automotive Data Traffic towards the Edge Cloud” *Proceedings of the 20th ITG-Symposium in Photonic Networks 2019*, 2019

[8] C. Fraleigh, F. Tobagi, and C. Diot. ”Provisioning IP backbone networks to support latency sensitive traffic.” *IEEE INFOCOM 2003. Twenty-second Annual Joint Conference of the IEEE Computer and Communications Societies (IEEE Cat. No.03CH37428)*. Vol. 1. 2003, pp. 375–385.

[9] M. Alasmar, R. Clegg and N. Zakhleniuk, and G. Parisis. ”Internet Traffic Volumes Are Not Gaussian—They Are Log-Normal: An 18-Year Longitudinal Study With Implications for Modelling and Prediction”, *IEEE/ACM Transactions on Networking*, vol. 29, no. 3, pp. 1266–1279, June 2021. doi:10.1109/TNET.2021.3059542, [arXiv:2007.10150].

[10] F. Feller. “An Optimization-Heuristic Approach to Dynamic Optical Bypassing”. *13th ITG Fachtagung on Photonic Networks*. May 2012.

[11] U. Bauknecht. ”A genetic algorithm approach to virtual topology design for multi-layer communication networks”. *Proceedings of the Genetic and Evolutionary Computation Conference (GECCO ’21). ACM*, pp. 928–936. [doi:10.1145/3449639.3459379]

[12] D. Willsch, M. Willsch, C. D. G. Calaza, F. Jin, H. De Raedt, M. Svensson and K. Michielsen, “Benchmarking Advantage and D-Wave 2000Q quantum annealers with exact cover problems,” *Quant. Inf. Comput.* ***21****, 2022, 141*, [arXiv:2105.02208.

[13] D-Wave. ”QPU Solver Datasheet: Annealing Implementation and Controls”. *D-Wave Online Manual*, (visited on 01/12/2022).

[14] T. Honjo et al. “100,000-spin coherent Ising machine”. *Science Advances* 7.40, 2021. doi: 10.1126/sciadv.abh0952

[15] F. Arute, K. Arya, R. Babbush, et al. ”Quantum supremacy using a programmable superconducting processor.” *Nature* 574, pp. 505–510 , 2019. [doi:10.1038/s41586-019-1666-5]